Astron. Astrophys. 334, 670–677 (1998)

ASTRONOMY
AND
ASTROPHYSICS

Localised, high-speed flows within the hydrogen-deficient planetary nebula Abell 78

J. Meaburn[1], **J.A. López**[2], **M. Bryce**[1], **and M.P. Redman**[1]

[1] Department of Physics and Astronomy, University of Manchester, Oxford Road, Manchester M13 9PL, UK
[2] Instituto de Astronomía, UNAM, Apdo. Postal 877, Ensenada, B.C. 22800, México

Received 24 December 1997 / Accepted 24 February 1998

Abstract. The remarkable velocity structure of the different components of the hydrogen-deficient planetary nebula Abell 78 have been revealed by obtaining spatially resolved profiles of the [O III] 5007Å line with the Manchester echelle spectrometer combined with the 2.1 m San Pedro Mártir telescope.

The outer, diffuse, hydrogen-rich, 124″ diameter shell is expanding radially at 40 $\mathrm{km\,s^{-1}}$. The irregular, knotty, hydrogen-deficient 89″ × 52″ inner shell has a similar overall expansion velocity but more complex kinematical structure. Similar to A 30, velocity 'spikes' are found in the position-velocity arrays of [O III] 5007Å profiles from the inner shell. These extend to a further -140 km s^{-1} than the radial velocity of the approaching side of this inner shell.

The [O III] 5007Å bright, hydrogen-deficient core knots are distributed throughout an elongated disk expanding at ≈ 25 km s^{-1}. There is kinematical evidence that 'polar bullets' are being ejected perpendicularly to this central feature at 380 km s^{-1}. Altogether 'velocity spikes' and other high-speed knots in the pv arrays of [O III] 5007Å profiles are found over a 455 km s^{-1} range of radial velocities.

Many of the kinematical phenomena are considered to be a consequence of the mass-loaded, shocked, wind from the central star.

Key words: planetary nebulae: individual: Abell 78 – ISM: kinematics and dynamics – ISM: jets and outflows

1. Introduction

Abell 78 (A 78) and the similar A 30 have been shown (Jacoby 1979; Jacoby & Ford 1983; Harrington 1996) to be members of a rare group of hydrogen-deficient planetary nebulae (PNe) which have evolved well beyond the phase where they ejected the hydrogen-rich envelopes that are so characteristic of the large majority of PNe (Abell 1966). The youngest galactic example yet found of this hydrogen-deficient class of PNe is A 58 (Pollacco et al 1992).

Both A 78 and A 30 have thin, nearly spherical, outer shells of hydrogen-rich gas, surrounding irregular [O III] 5007Å emitting inner shells (Borkowski et al 1993) emanating from knotty, bright, hydrogen-deficient nebular cores around O VI sequence stars. Iben et al (1983) have suggested that such stars have experienced a final thermal pulse after having achieved the white dwarf configuration typical of the majority of PNe central stars.

It was the discovery in HST images of cometary structures around the central knots that has heightened interest in both A 30 and A 78 (Borkowski et al 1993, Borkowski et al 1994, Borkowksi et al 1995, Harrington 1996). Convex arcs are present, orientated away from the central stars. Their presence immediately suggests that particle winds from the stars are over-running slow-moving globules. This interpretation is consolidated by the discovery of soft X-ray emission from the core of A 30 (Chu & Ho 1995) which indicates the presence of the attendant, high-Mach number bow-shocks. Also IUE spectral observations (Kaler et al 1988) of the central star of A 78 indicate the presence of a particle wind with a terminal velocity of $V_* = 3670$ $\mathrm{km\,s^{-1}}$ and a mass-loss-rate $\dot{M}_* = 4 \times 10^{-9}\,\mathrm{M_\odot\ yr^{-1}}$. Werner and Koesterke (1992) give $\dot{M}_* = 2.5{\times}10^{-8}\,\mathrm{M_\odot\ yr^{-1}}$ with a similar terminal velocity. The GHRS (HST) spectral observations of Harrington et al (1995) reveal directly that this wind is mass-loaded (Hartquist & Dyson 1993, Dyson et al 1993). Furthermore, they find absorption velocity components in the C IV 1548 & 1551 Å lines out to -385 km s^{-1} with respect to the systemic radial velocity. High-speed, outflowing, ionized gas is indicated.

Kinematical observations (Meaburn & López 1997) strengthened the view that wind-driven flows are ubiquitous throughout A 30. In particular, the discovery of $\pm\ 200$ $\mathrm{km\,s^{-1}}$ 'velocity spikes' in the position-velocity (pv) arrays of [O III] 5007Å line profiles over the edges of the irregular shells surrounding the bright core is direct evidence of the presence of mass-loaded flows possibly driven by a fast wind from the central star (though see Sect. 4).

More limited kinematical observations of A 78, with a scanning Fabry-Perot interferometer, have been reported briefly (Clegg et al 1992). They find an ≈ 30 km s^{-1} expansion velocity of the system of central knots and ± 100 km s^{-1} radial velocities for 'bullets' being emitted from this core.

The kinematical structure of the hydrogen-deficient, knotty core and irregular, [O III] 5007Å bright, inner shell as well as the outer, hydrogen-rich shell of A 78 have now been in-

Send offprint requests to: Professor J. Meaburn

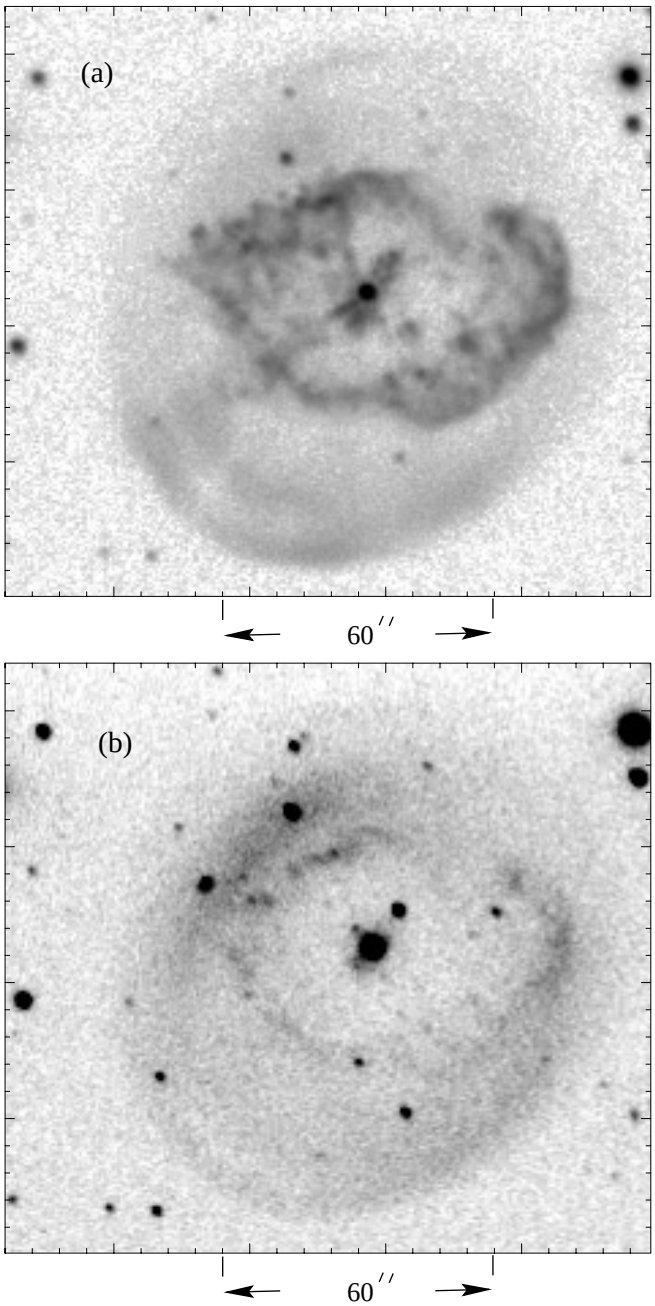

Fig. 1. a An [O III] 5007Å image of A 78. **b** An Hα and [N II] 6584Å image of A 78.

vestigated comprehensively by making spatially resolved spectral observations with the Manchester Echelle spectrometer (MES) combined with the San Pedro Mártir telescope. A distance to A 78 of 1.5 kpc will be used throughout this paper (Harrington et al 1995).

2. Observations and results

Both the imagery and the kinematical observations were obtained on the 6-9 November 1996 with the MES (Meaburn et al. 1984) at the f/7.9 focus of the 2.1m San Pedro Mártir UNAM telescope. A Tektronix CCD with 1024 $\times$ 1024, 24 μm, square pixels was the detector.

2.1. Imagery

In its imaging mode a plane mirror replaces the echelle grating in MES and a clear area the slit. Four separate images of A 78 through a 60 Å bandwidth [O III] 5007Å filter, each with a 60 s integration, were selected where the effects of 'seeing' were $\leq 1''$. With two times binning in both dimensions the images were marginally under-sampled with the resultant 0.6″ square equivelent pixels. After the usual processing and alignment (using the Starlink software package CCDALIGN) these were added to give the image shown in Fig. 1a. For comparison a single (60 s integration) image through a 90 Å bandwidth filter that transmits both the Hα and [N II] 6584Å nebular emission lines is shown in Fig. 1b.

2.2. Longslit spectrometry

MES in its spectrometric mode has no cross-dispersion. For the present observations, a filter of 60 Å bandwidth was used to isolate the 114th order containing the [O III] 5007Å nebular emission line. Two times binning was employed in both the spatial and spectral dimensions. Consequently, 512 increments, each 0.60″ long, gave a total projected slit length of 5.12′ on the sky. 'Seeing' varied between 1-2″ during these observations. The two 24 μm wide pixels in the spectral direction correspond to 4.7 $\mathrm{km\,s^{-1}}$. In Fig. 2a the slit positions, Pos. 1-10, where profiles of the [O III] 5007Å line were obtained are shown against the [O III] 5007Å image of A 78. Those slit positions which intersect the knotty nebular core are shown against an enlargement of the same [O III] 5007Å image in Fig. 2b. The 150 μm wide ($\equiv 1.9''$ on the sky) slit was orientated EW to give lamp line profiles measured as $\equiv 10\ \mathrm{km\,s^{-1}}$. These slit positions are particularly well determined for the insertion of a plane mirror into the beam before the echelle grating of MES permits an image to be taken of the slit against that of the field being observed (see Meaburn et al. 1984). Integrations of 1800 s duration were obtained for all of the slit positions. Each was followed by a calibration spectrum of a Th/Ar arc. A continuous tungsten spectrum was also obtained to compensate for the variations in sensitivity over the echelle order. The spectra were wavelength calibrated to an accuracy of $\pm 1\ \mathrm{km\,s^{-1}}$ using the Figaro data reduction package at the Manchester Starlink data reduction facility.

Negative greyscale representations of the [O III] 5007Å pv arrays for slit positions 1, 3, 7, 8, 9 & 10, now for 143″ of the slit lengths (equal to the width of Fig. 2a) are shown in Figs. 3a-f respectively. Here, the motions of the outer, hydrogen-rich, and inner, hydrogen-deficient, shells are most apparent. Deep representations of the same [O III] 5007Å arrays for positions 3 and 7 are presented in Figs. 4a and b respectively to reveal the faint, but highest speed outflows.

The [O III] 5007Å profiles over the bright, central, knots can be seen most clearly in the contour maps plus negative

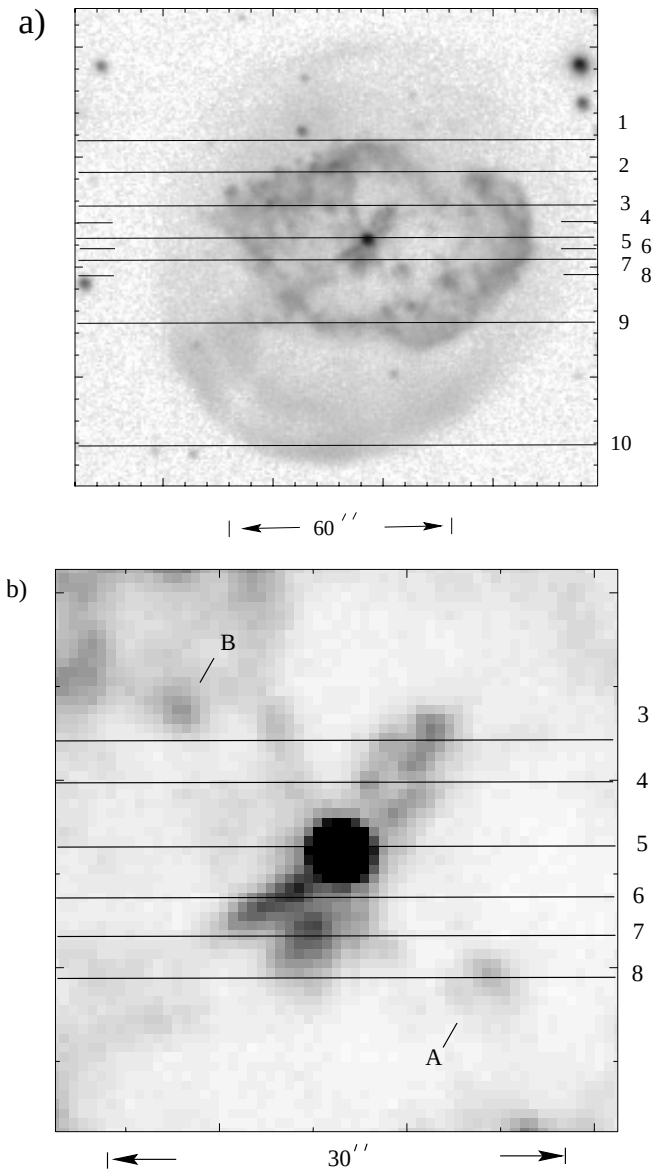

Fig. 2. a Slit positions 1-10 marked against the [O III] 5007Å image (in Fig. 1a) of A 78. **b** Slit positions 3-8 marked against an enlargement of the [O III] 5007Å image of the core of A 78. The velocity profile of the knot marked A is indicated in Fig. 3d. The counter-knot B is also identified.

greyscales in Figs. 5a-e for those parts intersected by slit positions 3, 4, 6, 7 & 8 respectively. The 30″ lengths of pv arrays depicted here are indicated in Fig. 2b. The pv array for slit position 5 is not shown for it is heavily contaminated by the continuous stellar spectrum.

3. New kinematical features

The images in Figs. 1a and b reveal clearly the separate regions of A 78. There is the 124″ (≡ 0.90 pc) diameter, somewhat ovoid, outer hydrogen-rich shell. This surrounds the irregular and knotty 89″ × 52″ (≡ 0.65 pc × 0.37 pc) hydrogen-deficient, [O III] 5007Å bright, inner shell (Fig. 1a) which contains the elongated (along PA 135°) knotty core on either side of the central star.

A faint extension from the core knots can be seen in Fig. 1a to extend along PA 135° out to the south-eastern edge of the outer shell. As for A30 (Meaburn & López 1997), the pv arrays of [O III] 5007Å profiles in Figs. 3, 4 and 5 reveal that each of these regions is characterised by distinctly different kinematical behaviour.

3.1. Outer hydrogen-rich shell

Approximate radial expansion of the diffuse, outer, hydrogen-rich (though still [O III] 5007Å emitting - see Fig. 1a) shell is indicated by the 'velocity ellipse' along slit position 1 (see Fig. 3a) which just misses the northern edge of the inner shell. This is confirmed by the partial ellipses occurring at both ends of all the slit positions 3, 7, 8 & 9 in Figs. 3b-e respectively and the near closure of the ellipse along slit position 10 in Fig. 3f over the southern edge of the outer shell. The separation of the two velocity components in the [O III] 5007Å profiles at the centre of the part of the outer shell covered by slit position 1 (Fig. 3a) is 68 ±3 km s^{-1}. Under the assumptions that the outer shell is spherical and expanding radially then an expansion velocity of $V_{EXP} = 40 \pm 3$ km s^{-1} is indicated.

A systemic heliocentric radial velocity for A 78 of $V_{SYS} = -22 \pm 2$ km s^{-1} is given by the mean of the heliocentric radial velocities (V_{HEL}) measured at both edges of the outer shell intersected by slit positions 1, 3, 7, 8 and 9.

3.2. Inner hydrogen-deficient shell

As expected from its complex morphology in Fig. 1a the kinematics of the inner shell are far more complicated than those of the more diffuse outer shell. Firstly there are many bright knots a few arcsec across in the pv arrays along slit positions 2-9 (see the examples in Figs. 3b-e). Many, but not all, have similar radial velocities to the split velocity components of the outer shell in their vicinity. However, several are either inside or outside this radial velocity range. The most extreme bright knot of this type is 3″ across and is intersected by slit position 8 (marked as A in Fig. 3d and 2b) and has $V_{HEL} = 76$ km s^{-1} (i.e. a radial velocity difference of 98 km s^{-1} with respect to V_{SYS}) but a halfwidth of only ≈ 16 km s^{-1}. This knot may be inside the inner shell and be directly associated with the core knots (Sect. 3.3).

The profiles along several of the pv arrays in Fig. 3 show that this inner shell is far from a simple radially expanding feature. Along slit position 9 in Fig. 3e there is a small bubble within the larger feature which is expanding radially at ≈ 50 km s^{-1}. A similar phenomenon is present (not shown here) along slit position 2 over the northern edge of the inner shell. Also the trends in radial velocity over the eastern extents of slit positions 7 & 9 (Figs. 3c and d) are reminiscent of those for individual lobes of bi-polar PNe.

Faint high-speed phenomena, which are very similar to the kinematic features in A 30 (Meaburn & López 1997), are

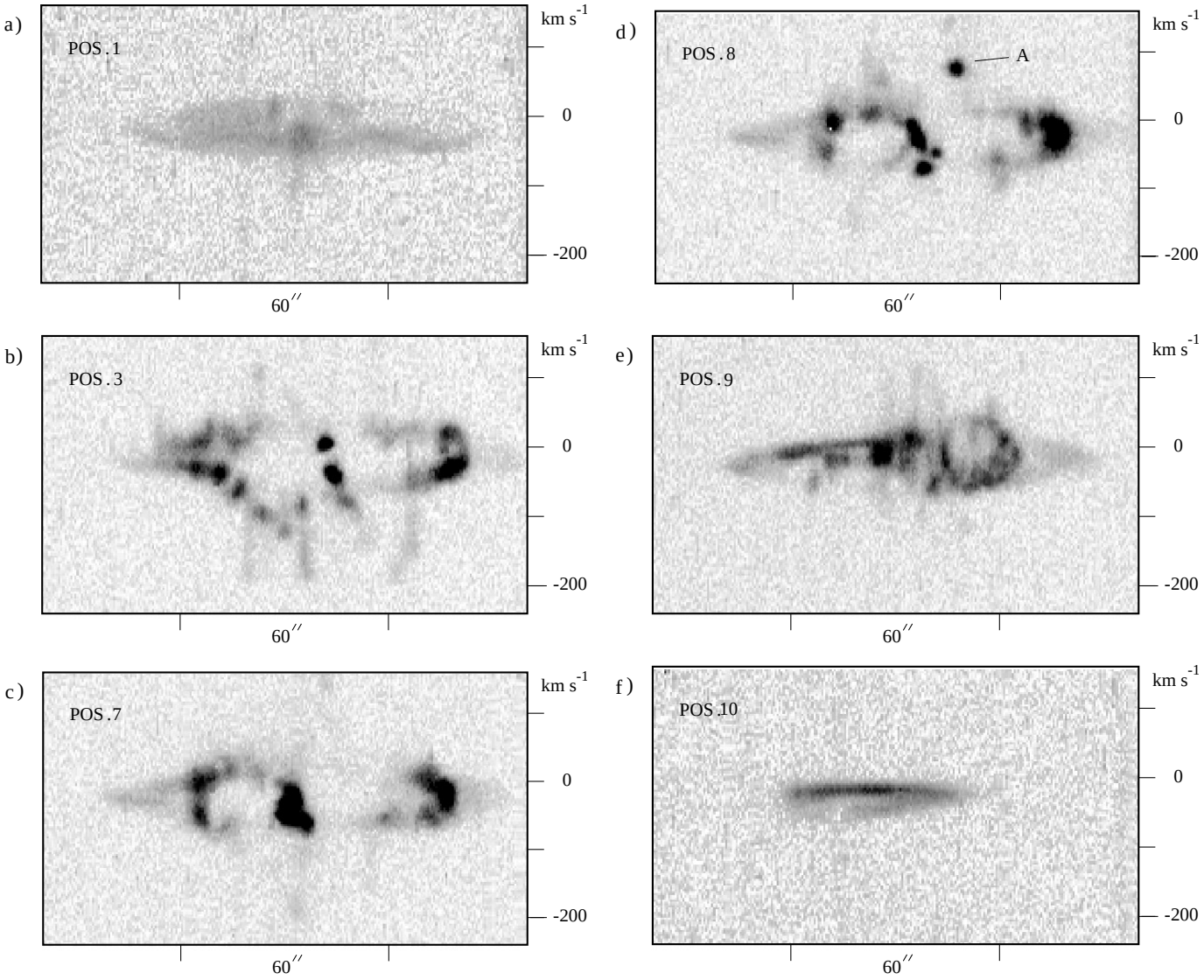

Fig. 3a–f. Negative greyscale representations of the pv arrays of [O III] 5007Å line profiles along slit positions 1, 3, 7, 8, 9 & 10 respectively. The vertical scale is heliocentric radial velocity. The total horizontal length is equal to the width of the image in Fig. 2a. The knot marked A along slit position 8 in **d** is also indicated in Fig. 2b.

present in the pv arrays over the inner shell of A 78. The most distinctive are the 'velocity spikes' that extend for ≈ -140 km s^{-1} from the approaching velocity components of the inner shell along slit position 3 (Figs. 3b and 4a). Curiously these 'spikes' have uniform brightnesses along their lengths and all finish abruptly at the same radial velocity ($V_{\rm HEL} = -195$ km s^{-1}). Similar 'spikes' to negative radial velocities can be seen along slit position 7 (Figs. 3c and 4b) but additionally, faint knots, at high positive radial velocity, are also present (i.e. up to $V_{\rm HEL} = 260$ km s^{-1}). The total range of radial velocities for the faint 'spikes' and knots in the pv arrays of [O III] 5007Å profiles is 455 km s^{-1}.

3.3. Core knots

The [O III] 5007Å bright, core knots distributed along PA 135° can be seen in Figs. 3 b-d and 5a-e to have a range of radial velocities within those for both the inner and outer shells. The more northern elongated feature, intersected by slit positions 3 and 4, emits bright [O III] 5007Å lines split by ≈ 45 km s^{-1} (Figs. 5a-b). reasonably symmetric around $V_{\rm SYS}$. The southerly feature covered by slit positions 6-8, has a somewhat more complex kinematic behaviour with three distinct velocity components present over radial velocity range of ≈ 50 km s^{-1} (Figs. 5c-f).

A line joining the point symmetric pair of knots marked A and B in Figs. 2b is perpendicular to the elongation of the core knots. The radial velocity difference of $+98$ km s^{-1} for knot A, with respect to $V_{\rm SYS}$, (see Sect. 3.2) is out of the range of that part of the pv array shown in Fig. 5e but confirms the measurements of Clegg et al (1992). Knot B was not covered by the present slit positions but must be the counter-knot to A observed by Clegg et al (1992) to have a radial velocity difference of -100 km s^{-1} with respect to $V_{\rm SYS}$.

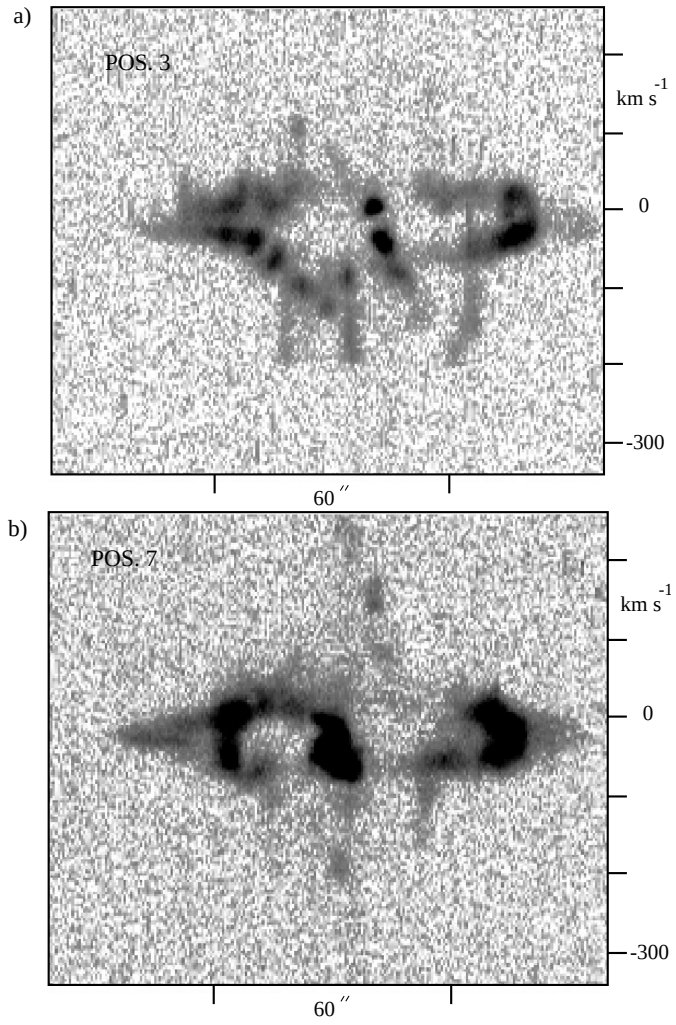

Fig. 4a and b. Negative greyscale representations of the same pv arrays shown in Figs. 3b,c for slit positions 3 & 7 but now printed deeply to reveal the faint, high-speed, velocity features. The radial velocity scale is heliocentric.

4. Discussion

It is clear that A 78 was a normal PN when it ejected a hydrogen-rich, diffuse, outer shell at 40 km s^{-1}. It then seems likely that, as the central star evolved to its OVI stage, it ejected both a hydrogen-deficient constraining disk and both a similarly deficient, but higher speed, knotty inner shell and 'bullets' in directions away from the plane of this disk. At some point in its evolution the star developed a fast particle wind but with a relatively low mass-loss-rate (see Sect. 1). However, significant mass-loading of this wind appears to be occurring within the nebular core as it sweeps up the evaporating gas from the photoionized surfaces of the dense central knots.

4.1. Kinematics

Neither the kinematics (Figs. 5a-e) nor the morphology (Fig. 2b) of the central, knotty, disk suggest that it is a simple, radially expanding, toroid whose axis is tilted at some angle θ to the plane of the sky. However, the width/length ratio of the whole feature is 0.26 which would give $\theta = 15^\circ$ if all the knots are contained within a circular disk viewed at this angle, in which simplistic case, the radial expansion of the system of core knots would be $\approx 25/\cos(15^\circ)$ km s^{-1} i.e. 26 km s^{-1}.

The kinematics and morphology of the inner shell (Sect. 3.2) must have been determined as it collided with, and swept-up, the thick outer shell (Sect. 3.1) for they both have similar expansion velocities. High-speed knots are seen throughout the interior of the inner shell. The most prominent are being ejected along the poles of the central disk (knots A and B in Fig. 2b). All of these 'bullets' are presumably travelling unrestrained within the volume of the inner shell.

The knots A and B are of particular interest if these are 'polar bullets' from a central star surrounded by a slowly expanding disk. If they are travelling outwards along the axis of this disk, tilted at $\theta \approx 15^\circ$, then their ejection speeds will be ≈ 386 km s^{-1} i.e. $100/\sin(15^\circ)$. This is remarkably close to the 385 km s^{-1} approaching absorption velocity component in the spectrum of the central star (Harrington et al 1995 and see Sect. 1). The receding and approaching strings of localised, faint, high-speed, knots near the nebular core in the pv array for slit position 8 (Fig. 4b) could be some manifestation of the same outflow of high-speed 'bullets' but orientated closer to the sight-line.

4.2. Dynamics

A range of dynamical explanations must be explored for the various kinematical and morphological phenomena observed here in A 78 and their counterparts in the very similar A 30 (Meaburn & López 1997). For instance, is the mass-loaded particle wind capable alone of forming the inner shell within the more diffuse and slowly expanding outer shell? If not, the inner shell may be the consequence of a succession of 'bullets' along different directions from the central star with ejection speeds of $\geq$380 km s^{-1}. The direct evidence presented here that such 'bullets' are being emitted in A 78 favours this mechanism. Bi-polar, symmetric, strings of knots in the PN Fleming 1 (López et al. 1993) and the knotty, bi-polar lobes of the PN KjPn 8 (López et al. 1997) are all considered to be persuasive evidence for the action of bi-polar, rotating, intermittent jets (strings of 'bullets') on the previously ejected nebular shells. The observations of the 'Hourglass' PN MyCn 18 are somewhat contradictory (Bryce et al 1997). Here the 'bullets' with $\geq$ 500 km s^{-1} speeds are found outside the apparent body of the nebula. The location of the knots and the open-ended morphology of the bipolar lobes in MyCn 18 may suggest that these knots have had very limited interaction with the surrounding nebula gas and are moving relatively unimpeded away from the main body of the PN.

The 'velocity spikes' reported here along the perimeter of the inner shell of A 78 and the similar ones in A 30 (Meaburn & López 1997) could either be some manifestation of the already mass-loaded wind as it collides with knots in the inner shell or be the consequence of high-speed 'bullets' as they plough through the outer shell.

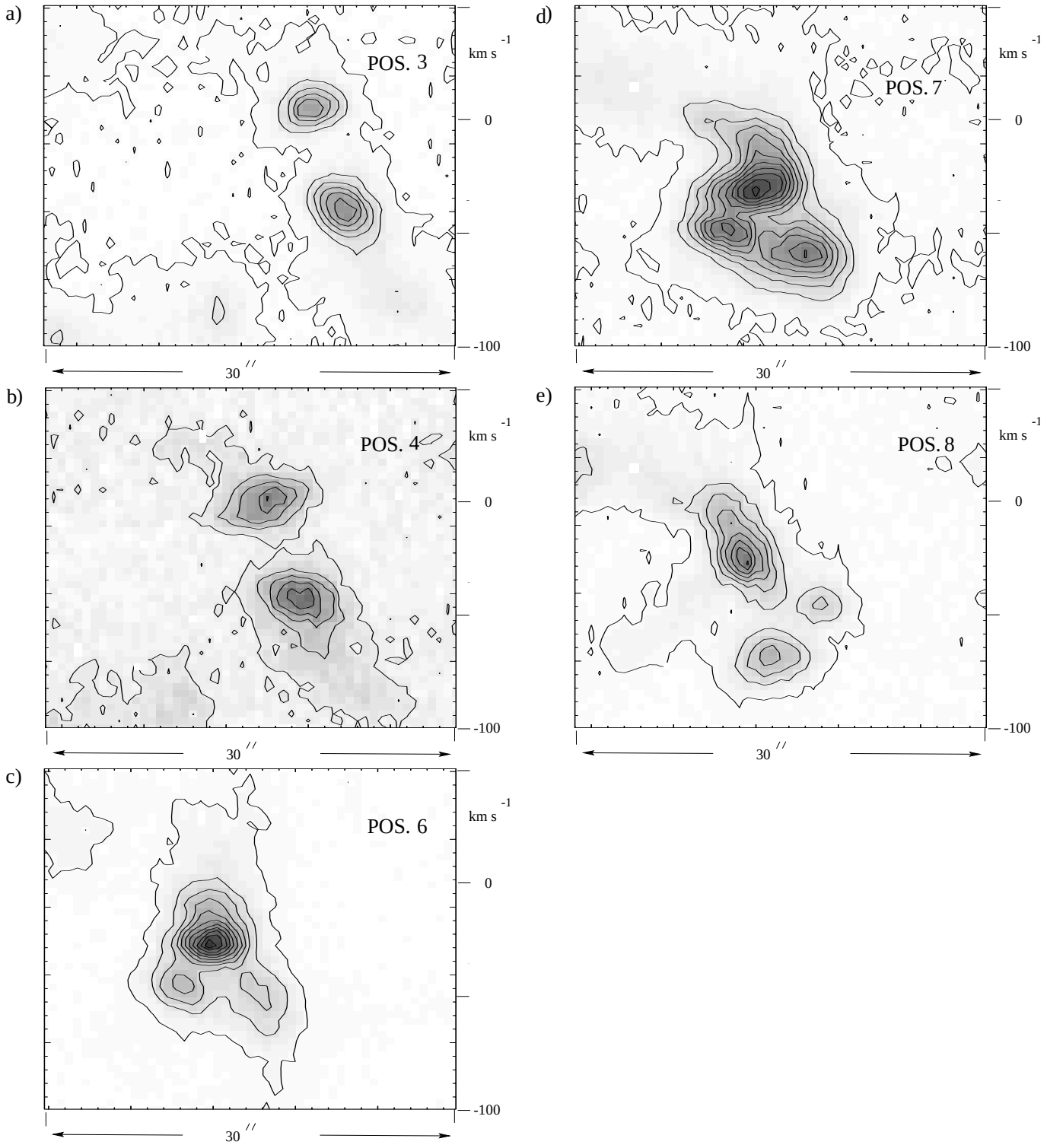

Fig. 5a–e. Contours, with linear intervals and negative greyscales, of the [O III] 5007Å pv arrays for those parts of slits 3, 4, 6, 7 & 8 that intersect the core knots of A 78. The 30″ lengths of the displays are shown in Fig. 2b. Again the radial velocity scale is heliocentric.

4.2.1. The core knots

The hydrogen deficient central region of A78 appears to be an excellent example of a directly observed mass-loaded flow (see Sect. 1). Mass-loaded flows have been reviewed by (Hartquist & Dyson 1993). The UV field and hypersonic tenuous wind from the central star respectively photoionizes and ablates material from adjacent globules. Unless they are transient structures, these core knots (Fig. 2b) must have dense neutral centres or else they would expand at the sound speed in the ion-

ized gas and lose their coherence as individual objects in less than a thousand years (Borkowski et al 1993).

The gas removed from the clumps is drawn out into a tail and is added to the wind via a possibly turbulent boundary layer. Recombinations are enhanced in the dense gas close to the clumps rendering them clearly visible in HST imagery. The subsequent energetics and dynamics of the flow are profoundly affected by this injection of mass which slows the flow down and increases its density. The flow energy (but not momentum) can be dissipated by enhanced radiative losses in the boundary layer between the wind and the newly injected clump material (Hartquist & Dyson 1993).

The ensemble of clumps (seen as the central bright knots in Fig. 1a ans 2b) may have been formed in an ejection event from the star. The clumps are located at around 0.1 pc from the star and have an expansion of around 26 km s^{-1} (Sect. 4.1), giving a kinematic age of $t_{\rm kin} \sim 10^3$ yr. This ejection event may be similar to that of A 58, the central star of which is thought to have undergone a nova-like event around 1919 and is now surrounded by knotty, hydrogen deficient material with velocities of $\approx 100\,{\rm km\,s^{-1}}$ detected (Pollacco et al 1992).

4.2.2. The hydrogen deficient inner shell

The velocity data presented in Sect. 3 shows that the hypersonic stellar wind must be decelerated to around $40\ {\rm km\ s^{-1}}$ at the edge of the hydrogen deficient shell. This shell can be formed in several ways. In the standard model (Dyson 1984), an isotropic hypersonic wind impinging on the ambient gas sets up a two shock flow pattern with an outer shock between the undisturbed circumstellar gas and the swept up shell; a contact discontinuity between this shell and shocked wind gas and a reverse shock between the shocked and unshocked stellar wind. For the conditions in A78, an energy conserving, pressure-driven, 'bubble' is expected in this classical picture since the dynamical timescale is far shorter than the cooling timescale. The predictions of a simplistic version of this model are obviously difficult to test against the observations of such a complex object as A 78. For one thing the formation of a pressure-driven inner shell would have to be considered within an already expanding outer shell. This model also assumes a uniform circumstellar medium which is obviously not the case in A 78.

Mass-loading and consequent cooling of the hypersonic stellar wind by radiative losses in the boundary layers around the central clumps of A 78 is therefore more likely to result in a momentum driven flow instead (Dyson 1994). However, note that, in their models of ultracompact H II regions, Dyson et al (1995) showed that a supersonic, momentum conserving, mass-loaded, flow can also generate a shell structure. They assume that mass is injected uniformly throughout the mass-loaded region and find that the flow can decelerate smoothly down to a Mach number of about 2. If the flow is slowed down to a velocity lower than about this, the flow undergoes a global shock but a shell will still be formed (Redman et al 1996). These models may adaptable to the conditions in the hydrogen deficient central regions of A78 where the stellar wind is decelerated by mass-loading. Of course, compared to the young massive stars that power ultracompact H II regions, PNe nuclei have less powerful winds and lower ionizing fluxes and the models of Dyson et al are ionization bounded which is clearly not the case for the inner shell in A78.

The momentum flux of the hypersonic stellar wind in A78 is $\dot{\mu_*} \equiv \dot{M}_* V_* \sim 10^{26-27}$ gm cm s^{-2}, depending on the mass-loss rate used (Sect. 1). It will be assumed that this momentum is conserved during mass-loading in the nebular core. Balancing the momentum input from the stellar wind, over the kinematic age of the inner shell, with the momentum of the inner shell gives, $\dot{\mu_*} t_{\rm kin} \approx 4\pi r_{\rm s}^2 \Delta r V_{\rm s} \rho_{\rm s}$; where $r_{\rm s} \approx 0.25$ pc, $\Delta r \approx 0.05$ pc, $V_{\rm s} \approx 40\,{\rm km\,s^{-1}}$ and $\rho_{\rm s}$ are, respectively, the radius, thickness, velocity and density of the shell. The number density in the inner shell implied by this simple calculation is less than 4 cm^{-3}, much lower than the $200 - 300\ {\rm cm^{-3}}$ estimated by Harrington et al (1995). The stellar wind momentum is therefore unable to generate the hydrogen deficient inner shell. As these alternative wind-driven mechanisms for generating the inner shell seem unlikely then ones that do not involve the stellar wind should be considered.

With a kinematic age of 6×10^3 yr the inner shell could of course just be the consequence of a short-lived ejection event from the central star at some time up to this age for it is likely to have decelerated during its lifetime. However, a further possibility is suggested by the present observations. Here the hydrogen-deficient inner shell has been formed by successions of high-speed 'bullets' ejected by the central star over a period of time and in various directions. The high-speed knots appear to be moving at $\lesssim 380$ km s^{-1} (see Sect. 4.1), a phenomenon that has also been seen in other PNe. Consider a high-speed globule with a uniform number density $n_{\rm g}$ and radius $r_{\rm g} \approx 10^{16}$ cm travelling at $v_{\rm g} \approx 300$ km s^{-1} through a uniform medium with density $n_{\rm i}$. Crudely, the globule will be disrupted after it has travelled through a column length l containing about the same amount of mass as the globule itself. If the globule is a hundred times denser than the surrounding nebula then it will be disrupted after travelling a distance $l \sim r_{\rm g}(n_{\rm g}/n_{\rm i}) \sim 10^{18}$ cm, which is approximately the radius of the hydrogen deficient inner shell. This will occur in a time of $\sim 10^3$ yr which is of the same order as a realistic age for the inner shell.

4.2.3. The 'velocity spikes'

The localised, faint, high-speed spikes (Sect. 3.2; Fig. 4) can be interpreted as either mass-loaded stellar wind being accelerated from the velocity of the edge of the inner shell (≈ 40 km s^{-1}) up to a cut-off of ≥ 250 km s^{-1} (i.e. 250/cos(ϕ) where ϕ is the angle of the collimated flow to the sight line) or else decelerating from this velocity to 40 km s^{-1}. The latter possibility is favoured since deceleration of the wind is required wherever further mass-loading is involved.

4.3. Conclusions

In light of these interpretations, the complex kinematical behaviour of the hydrogen-deficient inner shell can be suggested as follows. The hypersonic stellar wind is first decelerated by mass-loading from the inner core knots and undergoes a termination shock (Williams et al 1995 show that this shock can in fact be significantly weakened by the effects of mass-loading) bringing the velocity from several thousand km s^{-1} to several hundred km s^{-1}. Beyond the inner core, the mass-loaded, shocked, stellar wind continues as a weak, momentum conserving flow with the high-speed knots possibily dominant in the formation of the hydrogen-deficient inner shell as these knots are slowed and disrupted. The only manifestation of the mass-loaded wind at the periphery of the inner shell within this interpretation are the localised *decelerating* flows, seen here as 'velocity-spikes' around inhomogeneties.

Acknowledgements. We wish to thank the staff of the San Pedro Mártir observatory for their excellent assistance during these observations. JM is grateful to PPARC for funding the conversion of the Manchester echelle spectrometer for use on the San Pedro Mártir telescope. JAL acknowledges support from DGAPA-UNAM through projects IN 101495 and IN 111896.

References

Abell, G. O., 1966, ApJ, 144, 259.
Borkowski, K. J., Harrington, J. P., Tsvetnov, Z. & Clegg, R. E., 1993, ApJ, 415, L47.
Borkowski, K. J., Harrington, J. P., Blair, W. P. and Bregman, J. D., 1994, ApJ, 435, 722.
Borkowski, K. J., Harrington, J. P. & Tsvetanov, Z. I., 1995, ApJ, 449, L143.
Bryce, M., López, J. A., Holloway, A. J, Meaburn, J. 1997, ApJ, 487, L161.
Clegg, R. E. S., Devaney, M. N., Doel, A. P., Dunlop, C. N., Major, J. V., Myers, R. M. and Sharples, R. M., 1992, IAU Symp. 155, 'Planetary Nebulae' (Kluwer Academic Press) eds. Weinberger and A. Acker, P. 388.
Chu, Y. H. & Ho, C. H., 1995, ApJ, 448, L127.
Dyson, J. E., 1984, Ap&SS, 106, 181.
Dyson, J. E., 1994, in: Lecture Notes in Physics 431, 'Star Formation and Techniques in Infrared Astronomy' (Springer-Verlag) eds. Ray, T. P. and Beckwith, S. V. p. 93.
Dyson, J. E., Hartquist, T. W. & Biro, S., 1993, MNRAS, 261, 430.
Dyson, J. E., Williams, R. J. R. & Redman, M. P., 1995, MNRAS, 277, 700.
Harrington, J. P., Borkowski, K. J. & Tsvetanov, Z., 1995, ApJ, 439, 264.
Harrington, J. P., 1996, Proceedings of the 2nd International Colloquium on 'Hydrogen Deficient Stars', Bamberg, Germany, (Eds. C. S. Jeffrey & U. Heber), Astr. Soc. Pacific Conf. Series, 96, 193.
Hartquist, T. W. & Dyson, J. E. 1993, QJRAS, 34, 57.
Iben, I., Kaler, J. B. & Truran, J. W., 1983, ApJ, 264, 605.
Jacoby, G. H. 1979, PASP, 91, 754.
Jacoby, G. H. & Ford, H. C., 1983, ApJ., 266, 298.
Kaler, J. B., Feibelman, W. A. & Henrichs, H. F., 1988, ApJ, 324, 528.
López, J. A., Meaburn, J. & Palmer, J. W., 1993, ApJ, 415, L135.
López, J. A., Meaburn, J., Bryce, M & Rodríguez, L. F., 1997, ApJ, 475, 705.
Meaburn, J., Blundell, B., Carling, R., Gregory, D. E., Keir, D. F. & Wynne, C. G. 1984, MNRAS, 210, 463.
Meaburn, J. & López, J. A. 1997, ApJ, 472, L45.
Pollacco, D. L., Lawson, W. A., Clegg, R. E. S. & Hill, P. W., 1992, MNRAS, 257, 33.
Redman, M. P., Williams, R. J. R. & Dyson, J. E., 1996, MNRAS, 280, 661.
Werner, K. and Koesterke, L., 1992, in 'Atmospheres of Early-Type Stars' ed. U. Heber & C. S. Jeffrey (Berlin, Springer-Verlag) 288.
Williams, R. J. R., Hartquist, T. W., Dyson, J. E., 1995, ApJ, 446, 759.